American Mineralogist, Volume 65, pages 639-653, 1980

The effect of Fe and Mg on crystallization in granitic systems

MICHAEL T. NANEY

Chemistry Division, Oak Ridge National Laboratory[1]
Oak Ridge, Tennessee 37830

AND SAMUEL E. SWANSON

Geophysical Institute, University of Alaska
Fairbanks, Alaska 99701

Abstract

Single-step and multistep undercooling experiments using both Fe,Mg-free and Fe,Mg-bearing model granitic compositions were conducted to investigate the influence of mafic components on the crystallization of granitic melts. Crystallization of granite and granodiorite compositions in the system $NaAlSi_3O_8$–$KAlSi_3O_8$–$CaAl_2Si_2O_8$–SiO_2–H_2O produces assemblages containing one or more of the following phases: plagioclase, alkali feldspar, quartz, silicate liquid, and vapor. The observed phase assemblages are generally in good agreement with equilibrium data reported in the literature on the same bulk compositions.

With the addition of Fe and Mg to these bulk compositions six new phases participate in the equilibria (orthopyroxene, clinopyroxene, biotite, hornblende, epidote, and magnetite). However, crystalline assemblages produced in phase equilibrium and crystal growth experiments brought to the same final P–T–X_{H_2O} conditions are in general not equivalent. In crystal-growth experiments, nucleation of the feldspars and quartz is greatly inhibited in the presence of Fe and Mg. Indeed, plagioclase is the only tectosilicate to nucleate in the granodiorite composition. Mafic phases nucleate and grow outside of their thermal stability fields as defined by the equilibrium phase diagrams. This contrast in mineral assemblages between the equilibrium and crystal growth experiments is in marked contrast to the results obtained for Fe- and Mg-free compositions. Perhaps the addition of Fe and Mg has caused a breakdown of the Si–O framework in the melt, thereby promoting the more rapid nucleation of the ino- and phyllosilicates rather than the framework silicates.

Border zones of granitic plutons, commonly rich in mafic minerals, may result from the more rapid nucleation of mafic phases from the silicate liquid. These zones are thought to develop by early crystallization along the walls of the pluton. Our results suggest the mafic phases should nucleate more quickly than the feldspars and quartz and thus should enrich the early crystallization products in ferromagnesian minerals.

Introduction

Crystal-growth experiments were conducted to study the effects of iron and magnesium on crystallization processes in granitic magmas. Experiments were made by undercooling homogenized silicate liquids in single or multiple steps using both Fe,Mg-free and Fe,Mg-bearing model granitic compositions.

The phase equilibria relationships of the model granitic compositions have been previously studied. Whitney (1972, 1975) studied the Fe,Mg-free haplogranitic compositions, and Naney (1977) investigated the closely related Fe,Mg-bearing granitic compositions. Swanson (1977) studied the relation of crystal nucleation and growth rates to the development of granitic textures from silicate liquids generated from the Fe,Mg-free haplogranitic compositions. The success of Swanson's study and the availability of phase equilibria data to guide experimentation prompted this investigation.

At the outset it was expected that nucleation and growth of the felsic phases from the Fe,Mg-bearing

[1] Operated by Union Carbide Corporation for the U.S. Department of Energy under Contract W-7405-eng-26.

0003–004X/80/0708–0639$02.00

compositions would be similar to the behavior of these phases in the Fe,Mg-free haplogranitic compositions. Our objectives were to: (1) investigate the development of textures in granitic rocks by comparing growth from Fe,Mg-free compositions with growth from Fe,Mg-bearing compositions, and (2) evaluate kinetic factors important to crystallization of magmas (crystal nucleation and growth rates). The delay or complete inhibition of felsic phase nucleation and growth from the Fe,Mg-bearing compositions was unexpected.

We compare the crystallization of the mafic-free with mafic-bearing granitic systems and offer an explanation for the contrasting behavior. One implication of the inhibition of felsic phase growth for natural granitic melts is discussed.

Previous work

In an attempt to understand pegmatite genesis, Jahns and Burnham (1958) grew crystals from a hydrous silicate liquid. Natural samples of pegmatite and H_2O sealed in noble-metal capsules were heated to produce silicate liquids and were subsequently cooled to various subliquidus temperatures to study crystallization. Formal results of these experiments have not been reported. However, a photograph published by Wyllie (1963) illustrates the apparent success of these experiments.

Mustart (1969) found that crystals of albite up to 3 mm in length could be grown from a peralkaline melt in the system $NaAlSi_3O_8$–$Na_2Si_2O_5$–H_2O. Mustart (1972) used the technique of homogenization of the silicate gel plus H_2O charge above the liquidus, followed by crystallization at subliquidus temperatures. Substitution of $KAlSi_3O_8$ or SiO_2 for $NaAlSi_3O_8$ allowed potassium feldspar and quartz respectively to grow in place of albite.

Nucleation and growth kinetics of alkali feldspars from hydrous silicate liquids in the system $KAlSi_3O_8$–$NaAlSi_3O_8$–H_2O have been studied by Fenn (1972, 1977) following the method of Mustart (1972). Experiments were made with both H_2O-undersaturated and -saturated silicate liquids at 2.5 kbar. Alkali feldspars grew elongate parallel to the *a* crystallographic direction, with relative growth rates in the unit cell such that $a > c > b$. Crystal growth rates up to 6.8×10^{-6} cm/sec were measured parallel to *a*. Some experiments which were undercooled with respect to the liquidus for periods of 72 hours or more showed no signs of crystal nucleation. Because of the variability in this nucleation lag time (time between *T* drop to subliquidus value and crystal nucleation) it was not possible to determine the exact time over which growth took place, and therefore the measured crystal growth rates are minimum values. The morphology of the crystalline products were spherulitic except in experiments containing an aqueous vapor phase, which produced single isolated crystals at temperatures near the liquidus. Within the hypersolidus region the crystal growth experiments yielded products predicted by the equilibrium phase diagram.

Growth of plagioclase from hydrous silicate liquids has been studied in the system $NaAlSi_3O_8$–$CaAl_2Si_2O_8$–H_2O by Lofgren (1974a,b). Lofgren made both isothermal and step-cooling (periodic lowering of temperature by a prescribed amount) crystal growth experiments at 5 kbar. Morphology of plagioclase crystals was observed to change from a generally equant, tabular form at small undercooling values ($\Delta T = T_{\text{liquidus}} - T_{\text{experiment}}$) to skeletal, dendritic, and finally spherulitic crystal forms at the highest ΔT. Association of spherulitic growth textures with rapid cooling rates is well illustrated in photographs (Lofgren, 1974a). Spherulitic overgrowths produced during the temperature decrease at the termination of the experiment mantle the surfaces of tabular crystals. Lofgren (1974a) observed that nucleation incubation periods increased with the Na content of the system at small values of ΔT in isothermal crystal growth experiments. One experiment failed to produce crystals after six days at ΔT of 40°C. Experiments made with stepwise cooling profiles produced normally zoned plagioclase crystals analogous to those found in many natural occurrences (Lofgren, 1974a,b).

Lofgren and Gooley (1977) have grown feldspar crystals containing non-equilibrium intergrowths that texturally resemble perthite from melts in the system $NaAlSi_3O_8$–$KAlSi_3O_8$–$CaAl_2Si_2O_8$–H_2O. Experiments using linear cooling rates or stepwise cooling paths both produced plagioclase crystals intergrown with thin lamellae or patches of alkali feldspar near their outer margins. They attribute the plagioclase–alkali feldspar intergrowths to the formation of a boundary layer of melt enriched in alkali-feldspar-forming components rejected from the advancing plagioclase–liquid interface. The boundary layer develops in response to slow diffusion of alkali-feldspar-forming components in the melt relative to rapid growth of the adjacent plagioclase crystal and produces two changes advantageous to development of plagioclase–sanidine intergrowths. The presence of the boundary layer causes a breakdown of planar

plagioclase–liquid interfaces, resulting in a change from a tabular to dendritic growth habit for plagioclase. Further, the boundary layer eventually becomes sufficiently enriched in alkali-feldspar components for local crystallization of alkali feldspar to occur around the plagioclase dendrites.

Swanson *et al.* (1972) and Swanson (1977) studied crystal nucleation and growth from synthetic granite and granodiorite melts in the system $NaAlSi_3O_8$–$KAlSi_3O_8$–$CaAl_2Si_2O_8$–SiO_2–H_2O. Crystal growth rates of plagioclase, alkali feldspar, and quartz were found to vary as a function of ΔT of the experiment from 10^{-6} to 10^{-9} cm/sec. The highest growth rates were observed in experiments with H_2O-undersaturated compositions undercooled approximately 200°C. Maximum growth rates observed in the presence of an aqueous vapor phase are two orders of magnitude lower than those measured in H_2O-undersaturated experiments, and occur at larger undercooling ($\Delta T \simeq 400$°C). With the exception of the metastable persistence of glass (quenched silicate liquid) at subsolidus temperatures, crystal growth experiments produced phase assemblages consistent with the equilibrium phase diagram. Presumably this metastable glass would crystallize if experiments were continued for longer periods of time.

Several recent studies have dealt with crystal growth from mafic silicate liquids in the basalt–ultramafic compositional range. Textural simulation experiments have been made with model lunar basalts by a number of workers, including Lofgren *et al.* (1974) and Walker *et al.* (1976). Donaldson (1976, 1979) studied the development of crystal morphologies and delay in nucleation of olivine as functions of composition, superheating, undercooling, and cooling rate in mafic systems. Gibb (1974) studied crystallization of plagioclase from two silicate liquids of basaltic composition. Plagioclase nucleation from these melts was found to be a function of both the magnitude of ΔT and duration of the experiment. He showed that with slow constant cooling rates (0.05°C/hr) plagioclase and clinopyroxene will nucleate from melts of the compositions investigated at smaller ΔT than for faster cooling rates (10°C/hr).

Experimental techniques

Bulk compositions

Prior to making crystal growth experiments, equilibrium phase relations for the compositions of interest must be well known. The equilibrium data help to guide and interpret crystallization experiments. Equilibrium phase relations of two anhydrous simplified granitic compositions in each of the systems $NaAlSi_3O_8$–$KAlSi_3O_8$–$CaAl_2Si_2O_8$–SiO_2 and $NaAlSi_3O_8$–$KAlSi_3O_8$–$CaAl_2Si_2O_8$–SiO_2–$KMg_{1.35}Fe_{1.42}Al_{1.15}Si_3O_{11}$ with varying amounts of H_2O have been investigated at 8 kbar by Whitney (1975) and Naney (1977) respectively. The same four anhydrous compositions were used in this study.

Our synthetic granite and granodiorite compositions are shown in Table 1, together with Nockolds' (1954) average biotite–hornblende granite and hornblende–biotite granodiorite after which the synthetic compositions were modeled. The Fe- and Mg-free granite and granodiorite compositions are designated R1 and R5 respectively. The Fe- and Mg-bearing synthetic granite and granodiorite were prepared by mechanical addition of 10 weight percent of an 'anhydrous biotite' composition (M1) to both the Fe- and Mg-free granitic compositions, hence they are referred to as R1+10M1 and R5+10M1 respectively. The three basic anhydrous bulk compositions—R1, R5, and M1—were synthesized as coprecipitated gels

Table 1. Chemical compositions studied

	Biotite-Hornblende Granite (Nockolds, 1954)	Hornblende-Biotite Granodiorite (Nockolds, 1954)	Synthetic Granite (R1)	Synthetic Granodiorite (R5)	Synthetic Anhydrous Biotite (M1)	Synthetic Granite (R1+10M1)	Synthetic Granodiorite (R5+10M1)
				WEIGHT PERCENT OXIDES			
SiO_2	70.56	65.50	74.14	70.52	40.43	70.77	67.51
Al_2O_3	14.00	15.65	15.04	17.95	12.93	14.83	17.45
Fe_2O_3	0.91	1.63	-	-	24.44	2.44	2.44
FeO	2.41	2.79	-	-	-	-	-
MnO	0.06	0.09	-	-	-	-	-
MgO	0.48	1.86	-	-	11.90	1.19	1.19
CaO	1.63	4.10	1.49	3.91	-	1.34	3.52
Na_2O	3.56	3.84	3.70	4.33	-	3.33	3.90
K_2O	5.39	3.01	5.63	3.29	10.29	6.10	3.99
TiO_2	0.40	0.61	-	-	-	-	-
P_2O_5	0.10	0.23	-	-	-	-	-
H_2O+	0.50	0.69	-	-	-	-	-
				NORMATIVE EQUIVALENT			
Quartz	24.5	20.0	27.9	24.4		23.4	20.2
Orthoclase	31.7	17.8	33.3	19.4		36.0	23.6
Albite	29.9	32.5	31.3	36.6		28.2	33.0
Anorthite	6.4	16.4	7.4	19.4		6.6	17.5
$CaSiO_3$	0.3	0.9	-	-		-	-
$MgSiO_3$	1.2	4.6	-	-		3.0	3.0
$FeSiO_3$	3.0	2.9	-	-		-	-
Magnetite	1.4	2.3	-	-		-	-
Ilmenite	0.8	1.2	-	-		-	-
Apatite	0.3	0.5	-	-		-	-
Hematite	-	-	-	-		2.4	2.4
Corundum	-	-	0.2	0.2		0.3	0.3

by a technique modified after the procedure described by Luth and Ingamells (1965). Temperature *vs.* X_{H_2O} equilibrium relations for R1, R5, R1+10M1, and R5+10M1 at 8 kbar after Whitney (1975) and Naney (1977) are shown in Figures 1 and 2.

Experimental method

Internally-heated pressure vessels modified after the design of Yoder (1950) were used for the crystal growth experiments (Holloway, 1971). Temperature measurements were made with Inconel-sheathed Pt/Pt-10Rh thermocouples which were calibrated periodically in their normal experimental configuration against the melting points of gold (1062.5°C) and sodium chloride (800.5°C). The melting point data were corrected for pressure effects from the data of Akella and Kennedy (1971) and Clark (1959). Temperature measurements are estimated to be accurate to ±10°C. Pressure was transmitted to the samples by an argon medium, and was measured with maganin cells in conjunction with a Carey-Foster bridge. Pressure measurements are believed to be accurate to ±100 bars.

Experiments with the Fe- and Mg-bearing compositions were not buffered to maintain a predetermined oxygen fugacity. However, the experimental apparatus yielded oxygen fugacity values intermediate to the Ni–NiO and Mt–Hm oxygen buffer reactions. This was determined using capsules containing solid buffer reactants. Holloway (1973) also observed that the oxygen fugacity in an internally-heated pressure vessel with argon as a pressure medium is in this range. Chou (1978) has used the hydrogen fugacity sensor technique to determine the oxygen fugacity of similar vessels between the Ni–NiO and MnO–Mn_3O_4 buffers.

Samples were prepared by encapsulating carefully weighed amounts of freshly boiled, deionized, distilled water and dried silicate gel in platinum or $Ag_{60}Pd_{40}$ tubes which were sealed by welding. The Fe-bearing compositions were loaded only in $Ag_{60}Pd_{40}$ tubes to minimize loss of Fe to the capsule material. The water content of capsules is thought to be accurate to ±0.3 weight percent of the reported value.

Capsules were heated to 1200, 1150, 1100, or 1000°C at 8 kbar for 18 to 96 hours. At these temperatures most of the bulk compositions are above their respective liquidus and produce optically-homogeneous silicate liquids. Liquidus temperatures were not attained in experiments with the R1+10M1 and R5+10M1 systems containing less than 2 weight percent H_2O because the $Ag_{60}Pd_{40}$ alloy used for capsules began melting at or below the liquidus temperatures for these granitic compositions (Naney, 1977).

Following production of a silicate liquid, the temperature of the experiment was rapidly lowered to the desired subliquidus value. Samples were allowed to re-equilibrate at this new temperature for 2 to 10 days and were then either subjected to another temperature decrease (stepwise cooling in 50° or 100°C steps), or the experiment was terminated by turning off the furnace power and quenching the samples to room temperature. The time required to drop the temperature of an experiment from one isotherm to another ranged from 3 to 10 minutes, depending on the magnitude of the temperature decrease. At the termination of the experiment, the temperature dropped 300°C within 10 minutes and room temperature was reached within 20 minutes. Limitations of the gas intensifier system used to pressurize experiments did not permit temperature drops to be made isobarically. Consequently, the pressure commonly fell 100 to 500 bars during a temperature drop of 50–100°C. Immediately following temperature re-equilibration the pressure was readjusted to its previous value (8 kbar).

Multistep experiments with the R1+10M1 and R5+10M1 compositions were cooled from 1150°C in increments of 50° or 100°C. Experiments with the Fe- and Mg-free compositions were cooled in increments of 50°C starting from 1100°C. Single-step experiments were made at 8 kbar with one growth step of 50°C to 350°C. Note that the actual undercooling attained is a function of the H_2O content of the system (Figs. 1 and 2). Undercooling experienced by two samples of different H_2O contents but cooled to the same temperature is a function of the slope of the vapor-undersaturated liquidus curve.

Analysis of experimental products

After completion of an experiment the capsules were removed from the pressure vessel and examined for leaks. Capsules that showed no indication of leakage were opened and the contents examined under binocular and petrographic microscopes to study surface textures and determine the presence of crystalline phases and glass.

X-ray diffraction patterns were obtained from some powdered samples to confirm mineral identification and for unit-cell refinement of feldspars. A Norelco X-ray diffractometer was used for routine identification. Powder photographs obtained for

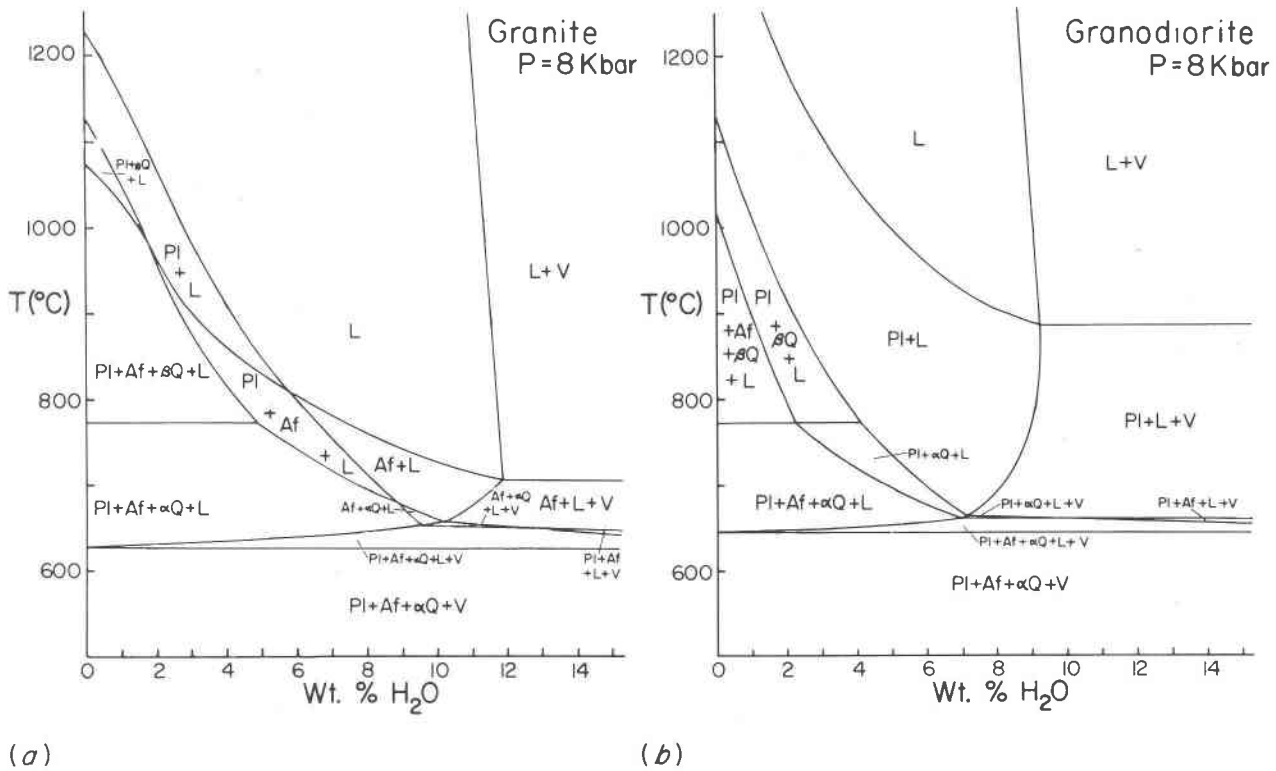

Fig. 1. Phase diagrams for Fe- and Mg-free bulk compositions at 8,000 bars, after Whitney (1975). Phase assemblages are shown as a function of temperature (T) and water content (weight percent H_2O) for the granite (a) and granodiorite (b). Pl is plagioclase, Af is alkali feldspar, Q is quartz, and L is quenched silicate liquid.

unit-cell refinements were made with a Nonius Guinier–de Wolff focusing camera used in conjunction with a fine-focus copper-anode X-ray tube. A spinel (a = 8.0833Å) internal standard was used in samples prepared for unit-cell refinement. Positions of diffraction lines on films were measured on an optical comparator with a precision of 0.001 mm (0.0005° 2θ). Measured peaks are thought to be accurate to ±0.010° 2θ or better. Unit-cell parameters were obtained using the least-squares computer program developed by Appleman and Evans (1973).

Electron microprobe analyses were made of crystals and glasses in selected samples with an Applied Research Laboratories model EMX-SM microprobe. Instrument conditions were as follows: beam-accelerating potential—15 kV (crystals and Fe,Mg-free glasses), 20 kV (Fe-,Mg-bearing glasses); sample current—0.02 microamp (crystals), 0.01 microamp (glasses); beam spot size—1 to 10 microns. These analytical conditions did not produce any noticable adverse effects (*i.e.*, alkali boil-off) in the glasses analyzed. An anhydrous glass of the mafic-free synthetic granite composition and synthetic plagioclase prepared by P. M. Fenn were used as standards for the analysis of the Fe- and Mg-free experiments. Analyzed natural minerals, glasses, and a synthetic glass were used as standards for analysis of the Fe- and Mg-bearing experiments. Data reduction was performed using a modified version of Colby's (1968) MAGIC IV computer program.

Experimental results

Nucleation

A number of crystal growth experiments failed to nucleate any crystals even after periods of up to 144 hours at subliquidus temperatures (Figs. 3 and 4). This nucleation lag time has also been observed in other granitic systems (Lofgren, 1974a; Fenn, 1977; Swanson, 1977) and is probably related to the slow approach to an equilibrium distribution of the atomic clusters in the silicate liquid prior to the beginning of nucleation (Turnbull and Fisher, 1949).

Compositions most commonly failed to nucleate crystals at low ΔT and in the presence of an H_2O-rich vapor phase. In general the Fe- and Mg-bearing systems more successfully nucleated crystals than did the mafic-free systems. Experiments with the Fe- and

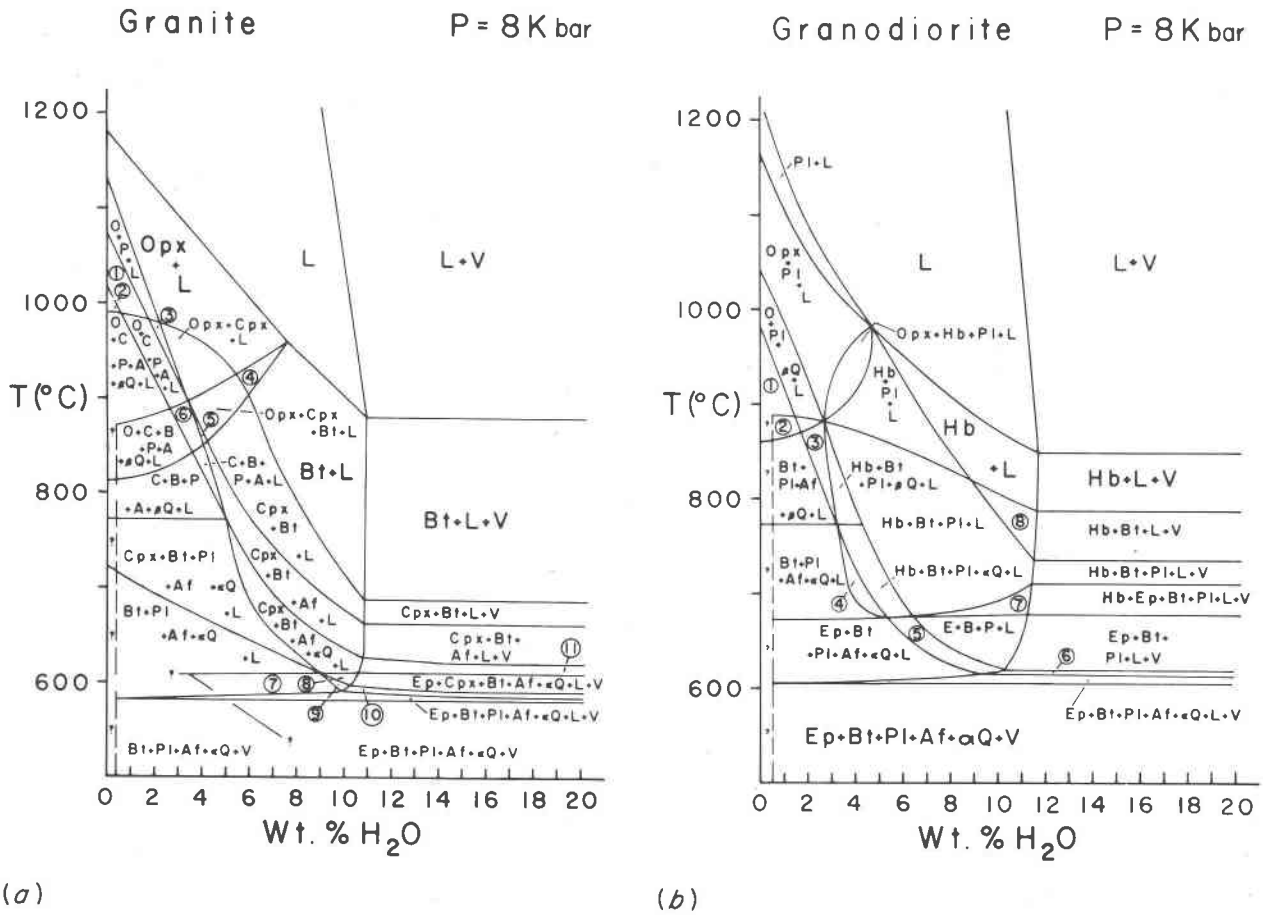

Fig. 2. Phase diagrams for Fe- and Mg-bearing bulk compositions, after Naney (1977). The symbols and abbreviations used on these phase diagrams are explained below. Dashed lines indicate uncertainty in position of stability limits for that phase. Opx = O = Orthopyroxene; Bt = B = Biotite; Cpx = C = Clinopyroxene; Hb = H = Hornblende; Ep = E = Epidote; Pl = P = Plagioclase; Af = A = Alkali Feldspar; αQ = Alpha-Quartz; βQ = Beta-Quartz; L = Silicate Liquid; V = Aqueous Vapor; ? = Queried field indicates that the beginning of dry melting is unknown and that the reaction relationships for the breakdown of biotite at low H_2O content are unknown.

Numbered fields shown in the granite diagram (a) represent the phase assemblages indicated: (1) Opx + Pl + Af + L; (2) Opx + Pl + Af + βQ + L; (3) Opx + Cpx + Pl + L; (4) Opx + Bt + L; (5) Opx + Cpx + Bt + Af + L; (6) Opx + Cpx + Bt + Pl + Af + L; (7) Ep + Bt + Pl + Af + αQ + L; (8) Ep + Cpx + Bt + Af + αQ + L; (9) Ep + Bt + Af + αQ + L; (10) Ep + Bt + Af + αQ + L + V; (11) Cpx + Bt + Af + αQ + L + V.

Numbered fields shown in the granodiorite diagram (b) represent the phase assemblages indicated: (1) Opx + Pl + Af + βQ + L; (2) Opx + Bt + Pl + Af + βQ + L; (3) Bt + Pl + βQ + L; (4) Hb + Bt + Pl + Af + αQ + L; (5) Ep + Bt + Pl + αQ + L; (6) Ep + Bt + Pl + αQ + L + V; (7) Hb + Ep + Bt + Pl + L; (8) Hb + Bt + L.

Mg-free compositions indicate that liquids of the synthetic granite composition (R1) are more reluctant to nucleate crystals than are those of the synthetic granodiorite composition (R5).

Crystal morphology

Morphologies of all crystalline phases were found to be strongly dependent on the magnitude of the undercooling imposed on a sample during a growth step, as expected from crystal growth theory (Kirkpatrick, 1975). The response of feldspar crystal morphology to changes in undercooling in the R1 and R5 compositions (Fig. 3) follows the same general pattern described by Lofgren (1974a). Briefly, experiments made at low undercooling (ΔT = 50 to 100°C) produced large tabular crystals up to 8 mm in length whereas crystals grown at larger ΔT have skeletal or dendritic morphology. Feldspar crystals have spherulitic morphology when growth took place at undercoolings ranging from ΔT = 100 to 350°C. Within this range of ΔT there is a gradual change in the appearance of spherulites. Undercooling values at the low end of this range produce rosettes composed of

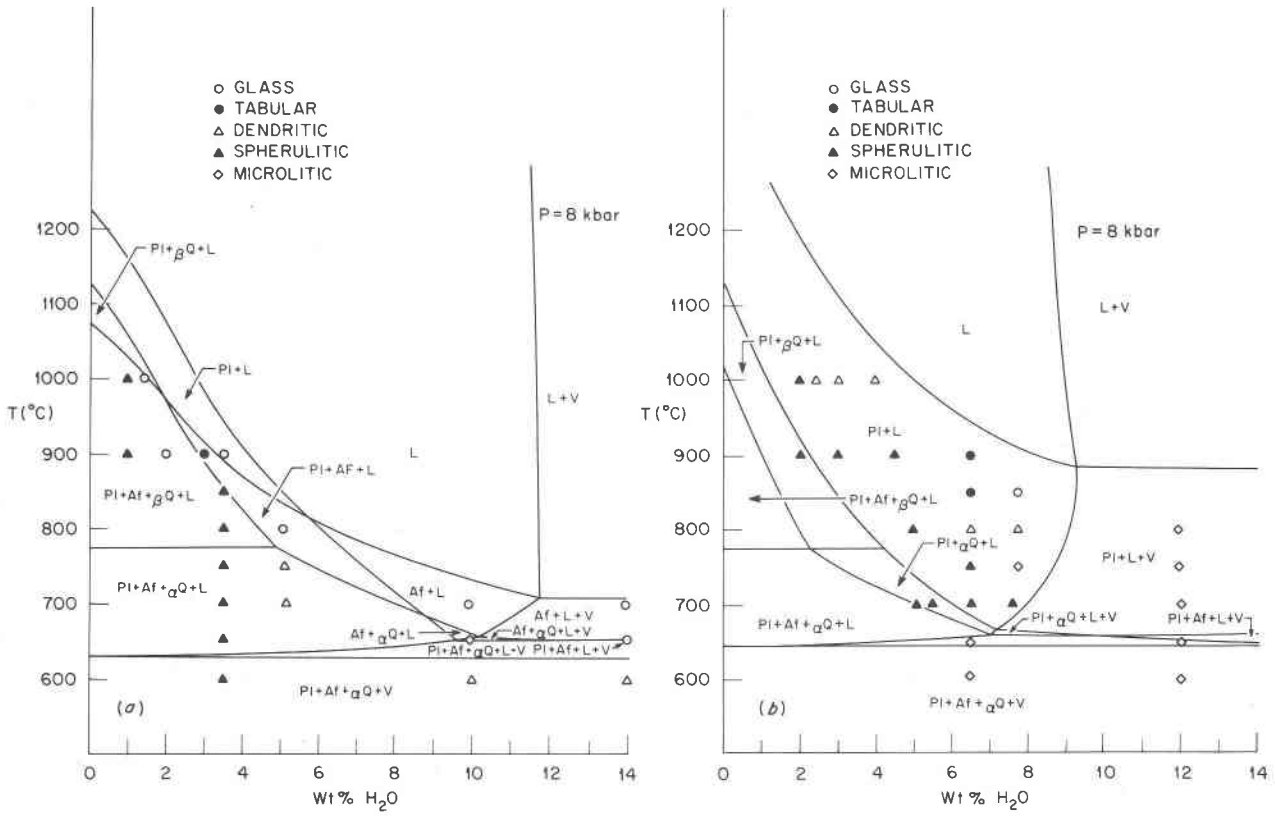

Fig. 3. Results of isothermal crystal growth experiments with the Fe- and Mg-free bulk compositions. Mineral assemblages are as indicated by the phase diagram except for those experiments that did not nucleate crystals. Experimental data used in this figure are available upon request from the authors.

large, faceted (up to 4 mm long) individual crystals radiating from a common center. The individual radiating crystals become smaller and more fibrous as the magnitude of undercooling increases, finally resulting in classical spherulites (Swanson, 1977). Quartz morphology in the mafic-free systems has been discussed in detail by Swanson (1977). In summary, quartz forms thin hexagonal plates, whose habit changes from euhedral, to skeletal, to dendritic crystals with increased ΔT.

The morphology of the mafic minerals, like those of the feldspars and quartz, is strongly dependent on the cooling history of the experiment. Ferromagnesian minerals in general exhibit the same growth pattern changes as those observed for the feldspars in this and other studies (Lofgren, 1974a; Fenn, 1977; Swanson, 1977). Euhedral crystals are observed at small ΔT values, hollow or skeletal crystals at slightly greater ΔT, and spherulitic or dendritic forms at the largest ΔT investigated.

In some experiments with the Fe- and Mg-bearing compositions there are prominent epitaxial overgrowths among ferromagnesian phases. Epitaxially-related growth pairs consisting of clinopyroxene crystals rimmed by orthopyroxene or orthopyroxene rimmed by clinopyroxene have been produced in different experiments with composition R1 + 10M1 by using the same bulk composition and changing the cooling path of the system (single-step *vs.* multistep crystallization). In addition, hornblende forms epitaxial overgrowths on clinopyroxene in experiments with the granodiorite composition. These overgrowths may have been promoted by chemical gradients near the crystal–liquid interface. Vapor bubbles occur as inclusions in a few clinopyroxene crystals or along crystal–glass interfaces, even though the bulk silicate liquid was undersaturated with respect to H_2O at the conditions of the experiment. Similar vapor bubbles were observed by Fenn and Luth (1973) in alkali feldspars crystallized from vapor-undersaturated silicate liquids. The heterogeneous nucleation of crystalline or vapor phases on crystal margins indicates local saturation of the silicate liquid with respect to a third phase at the crystal–liquid interface of a growing crystal. Local saturation is the result of rapid growth of the substrate crystal relative

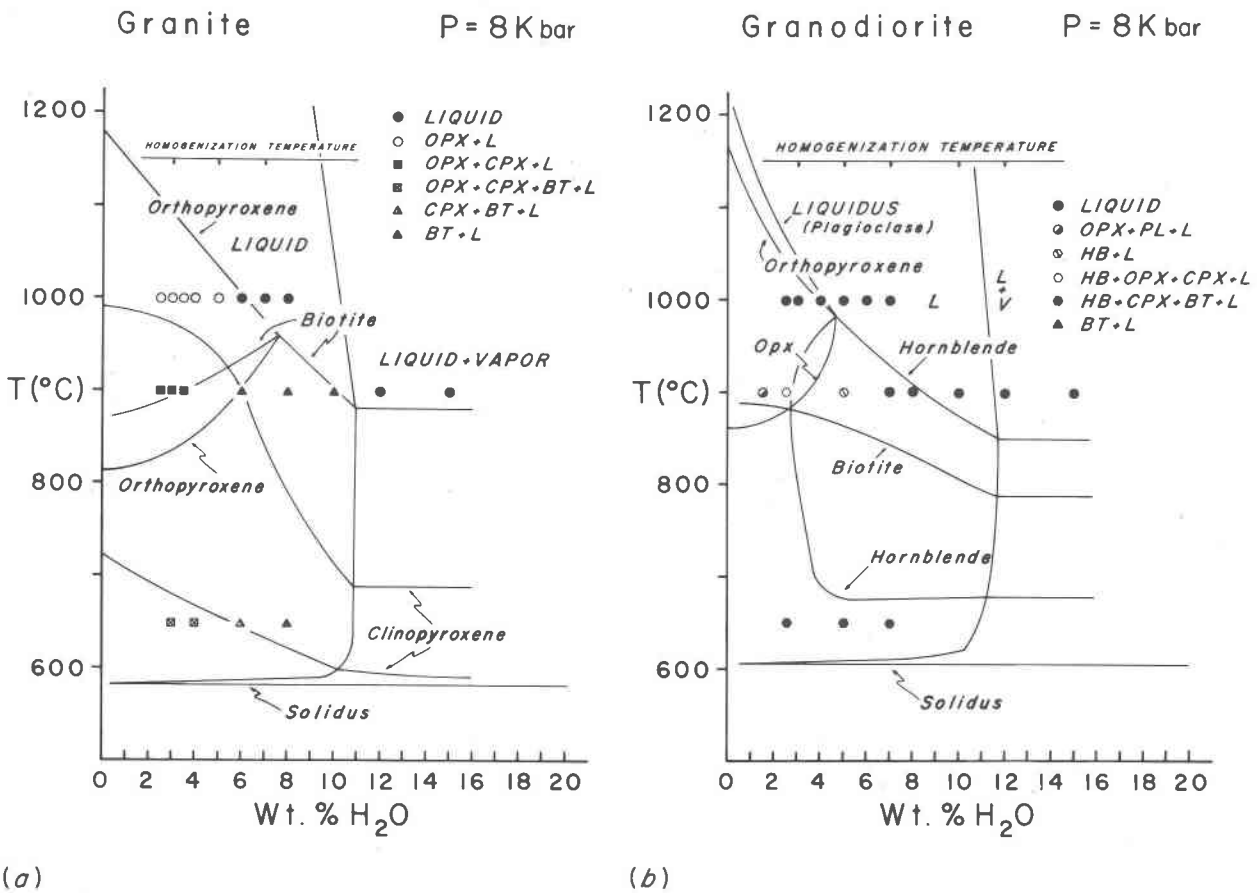

Fig. 4. Results of isothermal crystal growth experiments in the Fe- and Mg-bearing bulk compositions. Symbols indicate the phase assemblage observed in the experiments. Phase assemblage boundaries shown are those determined in phase equilibria experiments (Fig. 2) and are included for comparative purposes. Experimental data used in this figure are available upon request from the authors.

to the mobility of components rejected by the growing crystal.

Mineral assemblages in Fe- and Mg-free compositions

Single-step crystal growth experiments. Results of single-step crystal growth experiments with the Fe- and Mg-free compositions that nucleated crystals are consistent with the equilibrium phase diagram shown in Figure 1. Therefore, the phase diagram can be successfully used to predict the crystalline products of a crystal growth experiment. The results shown in Figure 3 duplicate the crystalline phase assemblage predicted by the phase diagram, *when* crystals do nucleate.

Although results of fractional crystallization experiments cannot in theory be predicted from the equilibrium diagrams, in practice our predictions have been quite successful. This success can be attributed to the degree of crystallization taking place in the experiments. In general a small volume ratio of crystals to silicate liquid is observed. Under these conditions the silicate liquid composition does not change significantly from the equilibrium composition.

Another test of equivalence between the results of phase equilibria and crystal growth experiments would be to determine the composition of the crystals grown from a single bulk composition at the same isotherm. Unfortunately, crystals grown in equilibrium experiments are very small and are not amenable to microprobe analysis. In the absence of microprobe data, X-ray powder diffraction patterns were obtained from crystal growth samples and their phase equilibria counterparts (Whitney, 1972, 1975). Results of the X-ray analysis indicate that corresponding feldspars in products of the two experimental methods have nearly identical unit-cell parameters. Table 2 contains an example of the unit-cell data obtained for feldspars from experiment R1-830 (Whitney, 1972) and the corresponding crystal growth experiment (426). Both experiments were

Table 2. Unit-cell refinements of feldspars

Sample Number	Alkali Feldspar		Plagioclase	
	R1-830	426	R1-830	426
a (Å)	8.517 ± .003	8.516 ± .002	8.184 ± .005	8.184 ± .001
b (Å)	13.017 ±.003	13.015 ±.002	12.879 ±.005	12.884 ±.001
c (Å)	7.177 ±.001	7.177 ±.001	7.127 ±.005	7.125 ±.001
α (° ')	90	90	93 19.3 ± 4.7	93 19.7 ± 0.6
β (° ')	115 58.7 ± 1.1	115 57.3 ± 0.9	116 28.0 ± 2.9	116 29.4 ± 0.6
γ (° ')	90	90	89 35.7 ± 4.7	89 34.5 ± 0.6
V (Å ^{3})	715.27 ±.25	715.17 ±.16	671.18 ±.45	671.14 ±.09
s.e	.019	.025	.036	.019
ref.	24/25	43/45	18/18	65/69

s.e. is the estimated standard error on the observation.

ref. is the number of peaks used in the refinement/number of peaks submitted.

Numbers below each of the unit cell refinements are the calculated standard errors.

Experiment R1-830 is a phase equilibria experiment from Whitney (1972) and 426 is a crystal growth experiment. Both experiments were made with the same bulk composition (R1 plus 3 weight percent H_2O) and crystallized at the same conditions (8000 bars, 700°C, 96 hrs).

crystallized at 700°C from the synthetic granite composition containing 3 weight percent H_2O. The phase assemblage produced in both experiments consisted of plagioclase, alkali feldspar, quartz, and silicate liquid. Results of the unit-cell refinements are, within the error of the refinement, identical.

Multistep crystal growth experiments. Multistep crystal growth experiments were made in an attempt to reduce the nucleation lag time and to study textures developed by crystallization at progressively lower temperatures. In the single-stage experiments, spherulites composed of some combination of plagioclase, alkali feldspar, and quartz were the dominant textural feature. Identification of individual phases within the spherulites was very difficult, and it was hoped that multistage experiments might produce crystals large enough to permit examination of the individual phases.

Results of the multistep experiments indicate that some of the difficulties encountered in the single-step experiments were overcome. Multistep experiments may allow the nuclei within the silicate melt time to readjust gradually to decreasing temperature, whereas the rapid large temperature drop used in single-step experiments may not allow sufficient time for nuclei to re-equilibrate with the melt. Two of the multistep experiments will be discussed in detail to illustrate the type of results obtained from experiments with the granite and granodiorite compositions.

At 8 kbar the granodiorite (R5) phase diagram contains a large plagioclase + silicate liquid field below the liquidus (Fig. 1b). Crystal growth in this system should produce plagioclase crystals followed at lower temperatures by quartz and alkali feldspar. A multistep experiment (504) was made using the R5 composition plus 4.0 weight percent H_2O. A portion of the experimental product is shown in Figure 5a. A single L-shaped, twinned crystal of zoned plagioclase is surrounded by two granophyric zones consisting of quartz, alkali feldspar, and plagioclase. The five zones within the plagioclase crystal can be correlated with crystallization at 1000, 950, 900, 850, and 800°C while the outer two granophyric zones represent crystallization at 750 and 700°C, as shown in Figure 5. The inner granophyric zone (750°C) composed of plagioclase, alkali feldspar, and quartz would be predicted to consist of plagioclase and quartz on the basis of the phase diagram (Fig. 1b). Coprecipitation of alkali feldspar with plagioclase at this temperature is probably a reflection of the extraction of plagioclase from the silicate liquid at higher temperature and consequent change in the liquid composition immediately adjacent to the plagioclase crystal face. The composition of the interface liquid is therefore effectively enriched with respect to quartz and alkali feldspar. Lofgren and Gooley (1977) reported similar interface enrichment and resulting intergrowths in the ternary feldspar system.

Nucleation problems encountered in the single-step crystal growth experiments can be circumvented in multistep growth because each growth zone in the crystal acts as a substrate for growth at the next lower temperature. Good minimum values of growth rate may be determined for the growth zones surrounding the core as contrasted with the more questionable growth rates measured in single-step experiments (Fenn, 1977; Swanson, 1977). Mean growth rates of the four zones which surround the core of the L-shaped plagioclase crystal range from 2.3×10^{-9} to 6.8×10^{-9} cm/sec (Fig. 5).

Results of quantitative electron microprobe spot analyses on the plagioclase and alkali feldspar in the L-shaped crystal of experiment 504 are shown in Figure 5. Normal zoning of the plagioclase is clearly indicated and each zone is homogeneous, at the scale of the electron microprobe analyses. Normally-zoned plagioclase crystals have also been produced by Lofgren (1974b) using a similar experimental method. He obtained qualitative electron microprobe analyses

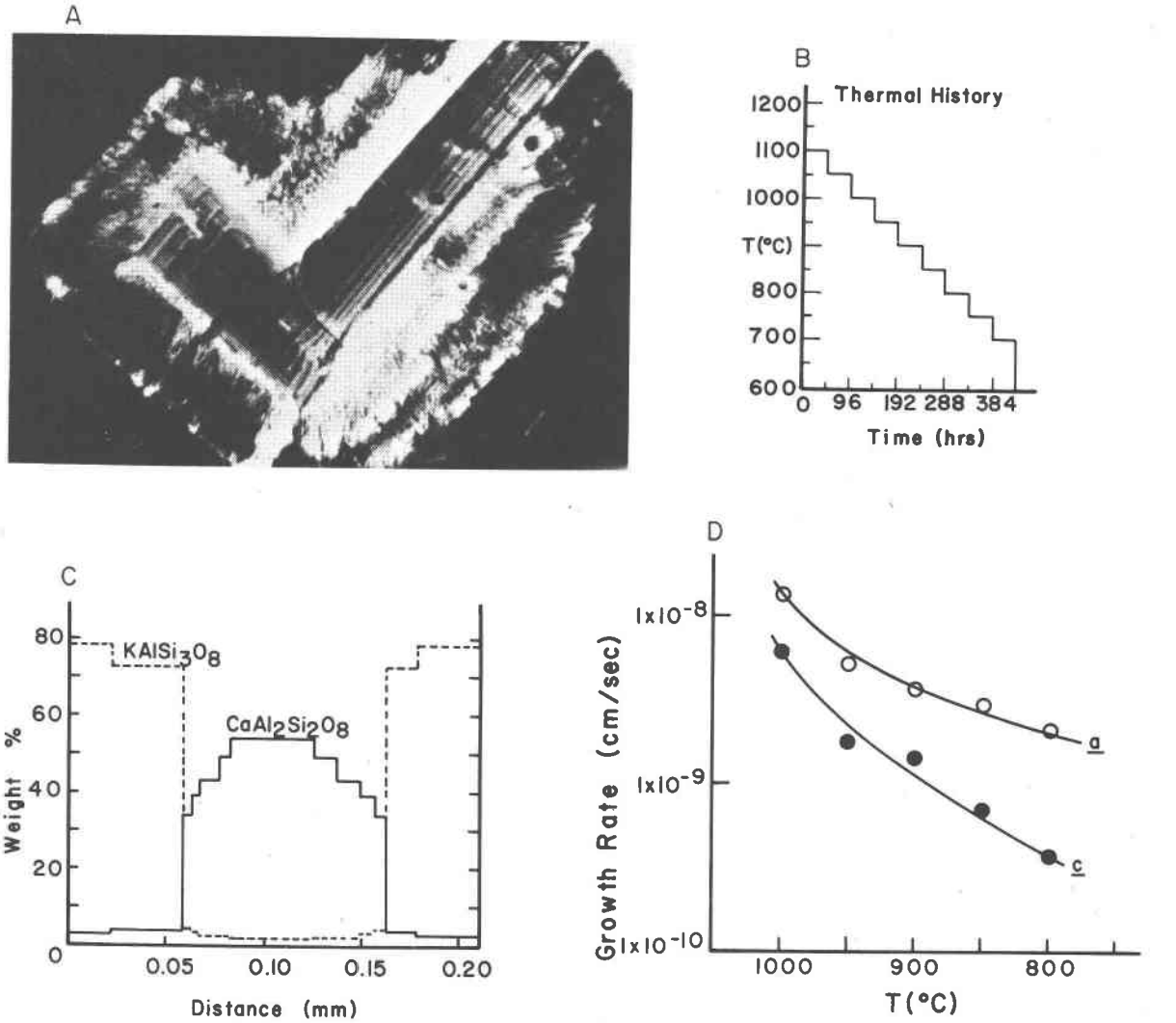

Fig. 5. Results of multistep crystal growth experiment 504 with composition R5 plus 4.0 weight percent H_2O. (A) Photomicrograph of L-shaped plagioclase crystal with five zones of growth corresponding to 1000°, 950°, 900°, 850°, and 800°C. Two zones of granophyric alkali feldspar, plagioclase, and quartz surround the plagioclase and represent growth at 750° and 700°C. Length of the small arm on the L-shaped plagioclase crystal is 0.29 mm. (B) Thermal history of experiment 504. (C) Electron microprobe analyses of L-shaped crystal perpendicular to the long arm of the L, showing the seven zones of growth. (D) Growth rate as a function of crystallographic direction (*a* axis and *c* axis) in the L-shaped plagioclase crystal.

from his samples that indicate the presence of reversed chemical zoning within some of the growth zones. Extinction patterns observed with polarized light in the plagioclase shown in Figure 5 suggest a similar reversed zoning pattern. However, this reverse zoning was not detected in the microprobe analyses of selected spots with a 5 micron beam diameter.

Equilibrium phase relations for R1 show a number of two- and three-phase assemblage fields between the liquidus and the four-phase (plagioclase + alkali feldspar + quartz + liquid) region (Fig. 1a). Each of these phase assemblages is stable over a relatively small temperature interval for a given H_2O content. Crystal growth experiments with the R1 composition should produce crystals of three different phases at rather small undercoolings ($\Delta T = 50$°C). This is in sharp contrast with results of crystal growth experiments with the synthetic granodiorite composition (R5), in which plagioclase was the only crystalline phase for over 200°C below the liquidus.

Crystal growth experiments with the R1 composition were not entirely successful, even when the multistep growth technique was used. Two experiments

with the granite composition (R1), containing 8 and 10 weight percent H_2O, were made concurrently with experiment 504 (Fig. 5) and neither produced any crystals. Though the ratio of crystals to silicate liquid within the alkali feldspar + liquid field (Fig. 1a) was expected to be small under these conditions, it was hoped that multistep cooling would generate nuclei of sufficient size to allow alkali feldspar growth at 700°C. Experiment 500 was prepared by adding 3 weight percent H_2O to the R1 composition. This experiment was also made concurrently with experiment 504. The rosettes shown in Figure 6 illustrate the dominant spherulitic growth form in experiments with the R1 composition, even when the multistep cooling technique is used. The equilibrium phase diagram for the granite composition indicates experiment 500 should have been in the subliquidus region at each growth step below 950°C. Thus six growth stages are expected in the rosettes shown in Figure 6.

Petrographic examination of the rosettes reveals three clearly defined zones and one poorly defined zone progressing inward from the spherulite margin. However, no identifiable zones corresponding to growth at 900° and 950°C were observed. Apparently nucleation was inhibited at 950° and 900°C, and the bulk of the spherulite formed at 850°C. Alternatively, crystallization of the central portion of the spherulite did take place at 950° and 900°C, but the boundaries between the high-temperature zones could have been eliminated by diffusion during annealing or recrystallization. Experiments with the R1 composition have demonstrated a tendency for sluggish nucleation, and because high-temperature growth zones within the L-shaped plagioclase crystal of experiment 504 are unaffected by annealing, nucleation was probably inhibited at 950° and 900°C in experiment 500.

Cores of the rosette-like spherulitic masses (experiment 500) appear on first inspection to be composed of subhedral plagioclase crystals radiating from a common center (Fig. 6). However, detailed examination reveals that these subhedral crystals are not homogeneous, and are made up of parallel filamentary needles. The bulk of the three outermost zones of the rosettes (800°, 750°, and 700°C growth zones) are composed of alkali feldspar ($Ab_{18}Or_{81}An_1$). Within the alkali feldspar are intergrowths of plagioclase and quartz (Fig. 6). These intergrowths are very similar to perthitic feldspars grown in experiments by Lofgren and Gooley (1977).

Summary

Crystal growth experiments with the Fe- and Mg-free (R1, R5) compositions yield the crystalline products predicted by the phase diagrams, except for experiments that failed to nucleate crystals or some intergrowths produced along a crystal–liquid interface. Nucleation lag times increased as ΔT decreased. No nucleation was observed in some experiments held for periods up to 144 hours at P–T conditions in the subliquidus–hypersolidus region. Many compositions failed to nucleate crystals (within this time frame) when their liquids were subjected to very small undercoolings.

The system failed to reach equilibrium for some multistep crystal growth experiments. In these exper-

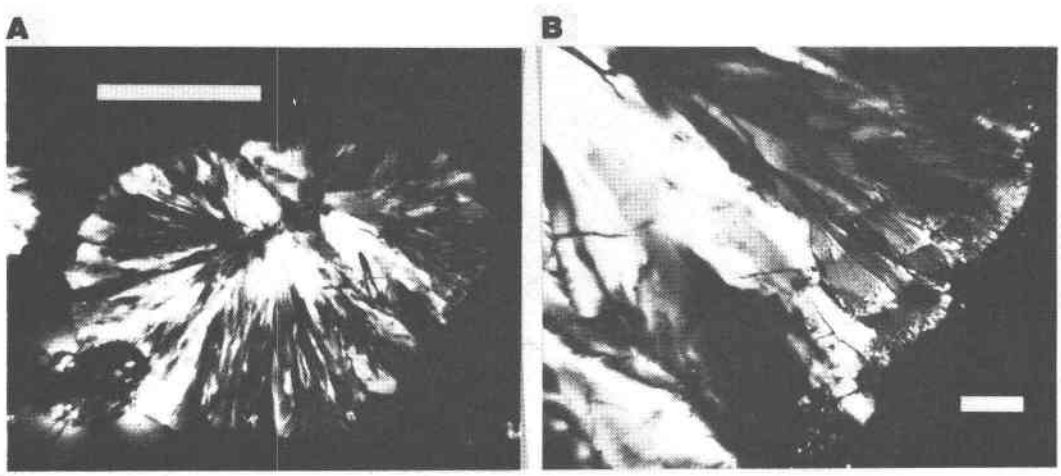

Fig. 6. Photomicrographs of experiment 500, R1 plus 3.0 weight percent H_2O. Thermal history is the same as experiment 504 (Fig. 5B). (A) Coarse-grained spherulites of alkali feldspar surrounded by quenched silicate liquid. White bar is 1.0 mm. (B) Close-up of spherulites in (A) showing intergrowths of plagioclase and quartz within the alkali feldspar in three growth zones. White bar is 0.1 mm.

iments, phases nucleate at higher temperatures than predicted from the equilibrium phase diagrams. The nonequilibrium phases always nucleate at the margin of a previously nucleated crystalline phase. The local change in liquid composition can be great enough to cause precipitation of a second, nonequilibrium phase at the boundary of a growing crystal.

Phase assemblages in Fe- and Mg-bearing compositions (R1+10M1, R5+10M1)

Phase assemblages in the products of crystal growth experiments with the Fe- and Mg-bearing compositions do not duplicate the assemblages of the phase diagrams in Figure 2. Most notably, alkali feldspar and quartz were not observed in the products of any crystal growth experiment with compositions R1+10M1 or R5+10M1. Plagioclase was observed in only one experiment with the granodiorite (R5+10M1) composition. However, in this experiment plagioclase appeared 250°C below its determined stability limit (plagioclase is the equilibrium liquidus phase at 8 kbar for the R5+10M1 composition).

Phases observed in crystal growth experiments with the synthetic granite (R1 + 10M1) include: glass (quenched silicate liquid), orthopyroxene, clinopyroxene, biotite, and magnetite. Phase-assemblage data resulting from crystal growth experiments with the R1 + 10M1 composition are shown in Figure 4a.

Results of crystal growth experiments with the R5+10M1 composition are shown on the T–X_{H_2O} phase assemblage diagram in Figure 4b. Phases observed in crystal growth experiments made with the granodiorite composition include: glass (quenched silicate liquid), orthopyroxene, clinopyroxene, hornblende, biotite, plagioclase, and magnetite. The presence of clinopyroxene is particularly interesting because equilibrium experiments (Fig. 2) predict its crystallization only from the granite composition. Alkali feldspar and quartz present in products of equilibrium experiments were not observed in crystal growth experiments.

In crystal growth experiments with either the R1+10M1 or the R5+10M1 composition, every ferromagnesian silicate phase was observed outside its stability field as defined by the phase diagram. Biotite is present in crystal growth experiments made at temperatures up to 100°C higher than its upper stability limit as shown on the equilibrium phase diagram. This biotite, apparently crystallizing above its stability limits, is interpreted to have grown during the quench. Quench biotite is sparse and nucleates only on the capsule wall. Biotite which is stable during the experiment is homogeneously distributed throughout the experimental product. Hornblende occurs in experiments containing lower H_2O contents and persists to lower temperatures than predicted by the equilibrium phase diagram. Clinopyroxene was observed at higher and lower temperatures relative to its equilibrium stability field. The occurrence of orthopyroxene is restricted to a smaller T–X_{H_2O} field than predicted by phase equilibria experiments. However, orthopyroxene was observed at a temperature well below its equilibrium stability field in a multistep experiment at 8 kbar with the R1+10M1 composition. However, in this case, orthopyroxene is mantled by clinopyroxene and thus cannot react with the silicate liquid. Epidote, a stable phase in equilibrium experiments made with both the R1+10M1 and R5+10M1 compositions, was not observed in the products of any crystal growth experiment.

Discussion of experimental results

Absence of feldspars and quartz from crystal growth experiments

Absence of or delayed nucleation of feldspars and quartz in crystal growth experiments produced phase assemblages which are strikingly different from those observed in equilibrium experiments made at the same P–T–X_{H_2O} conditions in the Fe- and Mg-bearing systems. In contrast, phase equilibria and crystal growth experiments with Fe- and Mg-free compositions show a high degree of correlation between phase assemblages produced in crystal growth and phase equilibria experiments made at the same P–T–X_{H_2O} conditions. Results of our crystal growth experiments plus phase equilibria results reported by Maaloe and Wyllie (1975) indicate that nucleation of alkali feldspar and quartz from a granitic liquid is very sluggish under laboratory conditions. Gibb (1974) reports that plagioclase nucleation is difficult in basaltic systems. Similar results are reported by Donaldson (1979) for the crystallization of olivine from basaltic melts. However, ferromagnesian minerals such as olivine generally nucleate faster than the tectosilicates (Gibb, 1974; Donaldson, 1979). In our crystal growth study alkali feldspar and quartz were not observed in the Fe- and Mg-bearing systems, even in experiments crystallized at low temperature (650°C). In addition, plagioclase was not present in any of the samples prepared from the synthetic granite composition that contains Fe and Mg. Depending on the H_2O content of the sample, these experiments

were undercooled with respect to the equilibrium liquidus for periods of 6 to 10 days. Some samples with low H_2O contents (less than 3 weight percent H_2O) were undercooled up to 250°C below the equilibrium upper stability limits of alkali feldspar and quartz as defined in Figure 2. Compared to nucleation incubation periods for these phases observed in the Fe- and Mg-free granitic compositions (Swanson, 1977), these periods should have been adequate for nucleation.

Effect of Fe and Mg on the structure of the silicate melt and crystallization kinetics

Addition of Fe and Mg to the simplified granitic compositions studied by Whitney (1975) and Swanson (1977) may modify the structure of the silicate liquid. Kushiro (1975) found that addition of MgO and FeO to simple silicate systems (containing 40 to 60 mole percent SiO_2) shifts eutectic liquid compositions to higher SiO_2 contents. He believes this composition shift is a reflection of structural changes occurring in the silicate melt. Addition of these cations presumably breaks Si–O bonds in the silicate liquid structure and makes the structure more like that of the silica-poor crystalline phase. In response to the change in silicate liquid structure, the stability field of the silica-poor phase is enlarged.

Results of phase equilibria experiments (Fig. 2) show that (when mafic phases are disregarded) the stability fields of assemblages consisting of combinations of plagioclase, alkali feldspar, quartz, and liquid are little changed from those found by Whitney (1975) in the Fe- and Mg-free granitic compositions (Fig. 1). Just as the addition of small amounts of Fe and Mg have little effect on the phase assemblage relations, these components (added in small amounts) probably have only minor effects on the structure of the silicate melt under equilibrium conditions. The presence of Fe and Mg in granitic liquids could restrict the size of regions within the melt which have framework-like structure, by breaking the Si–O bonds in the melt. If the size of these framework structures does not equal or exceed that necessary for formation of critical nuclei (Kirkpatrick, 1975), feldspar and quartz are inhibited from growing.

Preferential crystallization of mafic phases rather than feldspar and quartz may result from faster crystallization kinetics for the Fe- and Mg-bearing phases. Indeed, some authors relate the rapid crystallization of olivine and pyroxene relative to plagioclase in basic intrusives to the structural simplicity of the neso- and inosilicate relative to the tectosilicate (Wager, 1959; Hawkes, 1967). Since mafic phases crystallize before the tectosilicates in the systems we studied, it follows that after a temperature decrease to subliquidus values the formation of critical nuclei is faster for mafic phases than it is for tectosilicates.

The difference in nucleation rates may be related to size contrasts between critical nuclei of mafic and tectosilicate phases. If the critical nuclei of the tectosilicates are larger than those of the mafic phases they should take longer to form and thus allow earlier crystallization of the mafic phases. Formation of mafic nuclei may also be kinetically favored if the addition of Fe and Mg causes a breakdown of the Si–O framework structure in the melt. In either of these views rapid or preferential crystallization of mafic phases compared to tectosilicates is not related to the relative simplicity of mafic phase crystal structures, but rather to the rate of formation of critical nuclei in the melt.

Conclusions

Natural examples of rapid crystallization kinetics are well documented in the literature for mafic phases. Examples include the growth of olivine and pyroxene to the exclusion of plagioclase in the outer zones of pillow basalts (Bryan, 1972), development of mafic comb-layered zones where mafic phases nucleate faster than feldspars or quartz (Moore and Lockwood, 1973; Lofgren and Donaldson, 1975), and the rapid growth of olivine and pyroxene relative to plagioclase in the komatiites (Drever and Johnston, 1957; Arndt *et al.*, 1977). Indeed, although Bowen's reaction series is based on a particular basaltic bulk composition, it does illustrate the dominance of early-formed mafic phases, a crystallization sequence common for a variety of igneous rocks.

Our crystal growth experiments with the Fe- and Mg-bearing R5 + 10M1 composition illustrate the sluggish crystallization of tectosilicates relative to the mafic phases in granitic systems. Clinopyroxene is present in crystal growth experiments but is absent in equilibrium experiments made with this composition. This difference can be explained in terms of the supercooling of plagioclase in crystal growth experiments (250°C lower than in equilibrium experiments where plagioclase is the liquidus phase), and therefore lack of competition from plagioclase for calcium in the melt during growth of clinopyroxene. Early nucleation of plagioclase in crystal growth experiments would inhibit the growth of the other Ca-bearing phases, as illustrated by the absence of clinopy-

roxene from experiments that produce plagioclase. A similar argument may be made involving competition for potassium between alkali feldspar and biotite, resulting in crystallization of biotite rather than the tectosilicate. However, the absence of quartz from the crystal growth experiments cannot be explained by competition for components within the melt. Indeed, the early crystallization of mafic phases should promote the growth of quartz from the residual liquid, but quartz was not observed. Clearly, some factor in addition to competition for components in the silicate melt must inhibit the nucleation of tectosilicates. The observed nucleation of feldspars and quartz is best explained in terms of contrasting rates of critical nuclei formation in the silicate melt. This effect may be enhanced by competition between mafic and tectosilicate phases for components of the silicate liquid common to both phases.

Petrologic applications

Granitic plutons often show some sort of mineralogic zoning related to fractional crystallization of the mass of magma (Bateman *et al.*, 1963; Bateman and Chappell, 1979). The pattern of the zoning is often concentric about a late-crystallizing interior zone. Later intrusion of magma from the core into the previously crystallized magma often alters the concentric pattern. Mineralogic zonation in granitic plutons may also be asymmetric (Swanson, 1978), forming a continuous variation pattern from one side of the pluton to the other. In either case zoning patterns typically parallel the walls of the pluton. Boundaries between individual zones may be either gradational, reflecting subtle changes in the crystallizing magma, or sharp, due to intrusion of magma into previously crystallized zones.

A common feature of mineralogic zoning in granitic plutons is the presence of a border zone enriched in mafic minerals. Such a mafic border zone can be identified in a plot of the variation of mafic mineral content across the Tuolumne intrusive series (Fig. 7), a zoned granodioritic pluton in the eastern part of Yosemite National Park, California. One cause of mafic mineral enrichment near pluton contacts is contamination of magma by wall-rock material. However, field evidence indicates that no significant contamination by wall-rock material has occurred. In addition, the wall rocks are not of the proper composition to account for the variation observed in the intrusive sequence (Bateman and Chappell, 1979). Zoning in this pluton is thought to have developed by accretion of material crystallized from the magma at the margins of the magma chamber. This model requires the margins of the pluton to crystallize before the core, and therefore the minerals at the margin to nucleate sooner than minerals in the core. Heat losses from a magma to the surrounding wall rocks accelerate cooling at the margins of a magma chamber relative to interior zones. If inhibition of tectosilicate crystallization is significant at these "accelerated" but low cooling rates, then development of mafic-rich margins of this granitic pluton and others may be in part related to the more rapid nucleation of mafic phases relative to the feldspars or quartz observed at high undercooling in this study.

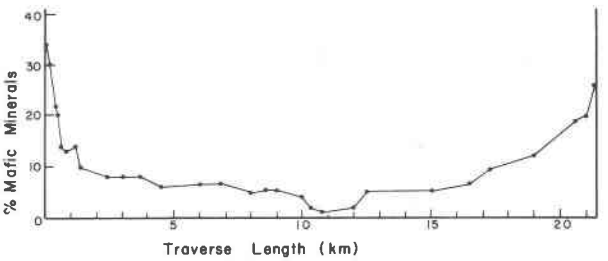

Fig. 7. Variation in mafic mineral (hornblende + biotite + magnetite + sphene) content across the Tuolumne Intrusive Series, a quartz diorite–granodiorite complex in Yosemite National Park (Traverse A–B of Bateman and Chappell, 1979). Total distance across the complex is slightly over 21 km.

Acknowledgments

We thank W. C. Luth and P. M. Fenn for much assistance and advice during the course of this study. P. R. Gordon skillfully maintained the experimental equipment. Among the individuals who have contributed to the ideas presented here through many stimulating discussions, the following deserve special mention: J. A. Whitney, J. G. Blencoe, J. C. Eichelberger, M. P. Taylor, P. Schiffman, G. E. Brown, J. G. Liou, J. D. O'Brient, and B. H. W. S. de Jong. The manuscript was improved by the careful reviews of E. Dowty and G. E. Lofgren. Financial support for this work was provided by NSF grants GA 1684 (R. H. Jahns and W. C. Luth) and GA 41731 (W. C. Luth, G. E. Brown, and W. A. Tiller). These studies were done while we were graduate students in the Tuttle–Jahns Laboratory for Experimental Petrology, Stanford University; the use of these facilities is gratefully acknowledged.

References

Akella, J. and G. C. Kennedy (1971) Melting of gold, silver, and copper—proposal for a new high-pressure calibration scale. *J. Geophys. Res., 76,* 4969–4977.

Appleman, D. E. and H. T. Evans, Jr. (1973) Job 9214: Indexing and least squares refinement of powder diffraction data. *Nat. Tech. Inf. Serv.,* U.S. Dept. Commerce, Springfield, Virginia, Document PB-216 188.

Arndt, N. T., A. J. Naldrett and D. R. Pyke (1977) Komatiitic and iron-rich tholeiitic lavas of Munro Township, northeast Ontario. *J. Petrol., 18,* 319–369.

Bateman, P. C. and B. W. Chappell (1979) Crystallization, fractionation, and solidification of the Tuolumne intrusive series, Yosemite National Park. *Geol. Soc. Am. Bull., 90,* 465–482.

———, L. D. Clark, N. K. Huber, J. G. Moore and C. D. Rinehart (1963) The Sierra Nevada batholith—a synthesis of recent work across the central part. *U. S. Geol. Surv. Prof. Pap. 414-D.*

Bryan, W. B. (1972) Morphology of crystals in submarine basalts. *J. Geophys. Res., 77,* 5812–5819.

Chou, I-M. (1978) Calibration of oxygen buffers at elevated *P* and *T* using the hydrogen fugacity sensor. *Am. Mineral., 63,* 690–703.

Clark, S. P., Jr. (1959) Effect of pressure on the melting points of eight alkali halides. *J. Chem. Phys., 31,* 1526–1531.

Colby, J. W. (1968) Quantitative microprobe analysis of thin insulating films. In J. Newkirk, G. Mallett and H. Pfeiffer, Eds., *Advances in X-ray Analysis,* vol. 2, p. 287. Plenum Press, New York.

Donaldson, C. H. (1976) An experimental investigation of olivine morphology. *Contrib. Mineral. Petrol., 57,* 187–213.

——— (1979) An experimental investigation of the delay in nucleation of olivine in mafic magmas. *Contrib. Mineral. Petrol., 69,* 21–32.

Drever, H. I. and R. Johnston (1957) Crystal growth of forsteritic olivine in magmas and melts. *Trans. R. Soc. Edinburgh, 63,* pt. II, 289–317.

Fenn, P. M. (1972) Nucleation and growth of alkali feldspars from synthetic melts (abstr.). *Trans. Am. Geophys. Union, 53,* 1127.

——— (1977) The nucleation and growth of alkali feldspars from hydrous melts. *Can Mineral., 15,* 135–161.

——— and W. C. Luth (1973) Hazards in the interpretation of primary fluid inclusions in magmatic minerals (abstr.). *Geol. Soc. Am. Abstracts with Programs, 5,* 617.

Gibb, F. G. F. (1974) Supercooling and the crystallization of plagioclase from a basaltic magma. *Mineral. Mag., 39,* 641–653.

Hawkes, D. D. (1967) Order of abundant crystal nucleation in a natural magma. *Geol. Mag., 104,* 473–486.

Holloway, J. R. (1971) Internally heated pressure vessels. In G. C. Ulmer, Ed., *Research Techniques for High Pressure and High Temperature,* p. 217–258. Springer-Verlag, New York.

——— (1973) The system pargasite–H_2O–CO_2: a model for melting of a hydrous mineral with a mixed-volatile fluid—I. Experimental results to 8 kbar. *Geochim. Cosmochim. Acta., 37,* 651–666.

Jahns, R. H. and C. W. Burnham (1958) Experimental studies of pegmatite genesis: melting and crystallization of granite and pegmatite (abstr.). *Geol. Soc. Am. Bull., 69,* 1592–1593.

Kirkpatrick, R. J. (1975) Crystal growth from the melt: a review. *Am. Mineral., 60,* 798–814.

Kushiro, I. (1975) On the nature of silicate melt and its significance in magma genesis: regularities in the shift of the liquidus boundaries involving olivine, pyroxene, and silicate minerals. *Am. J. Sci., 275,* 411–431.

Lofgren, G. E. (1974a) An experimental study of plagioclase crystal morphology: isothermal crystallization. *Am. J. Sci., 274,* 243–273.

——— (1974b) Temperature induced zoning in synthetic plagioclase feldspar. In W. S. MacKenzie and J. Zussman, Eds., *The Feldspars,* p. 362–376. Manchester University Press, Manchester, England.

——— and C. H. Donaldson (1975) Curved branching crystals and differentiation in comb-layered rocks. *Contrib. Mineral. Petrol., 49,* 309–319.

——— and R. Gooley (1977) Simultaneous crystallization of feldspar intergrowths from the melt. *Am. Mineral., 62,* 217–228.

———, C. H. Donaldson, J. J. Williams, O. Mullins, Jr. and T. M. Usselman (1974) Experimentally reproduced textures and mineral chemistry of Apollo 15 quartz normative basalts. *Proc. Fifth Lunar Sci. Conf.,* 549–567.

Luth, W. C. and C. O. Ingamells (1965) Gel preparation for hydrothermal experimentation. *Am. Mineral., 50,* 255–258.

Maaloe, S. and P. J. Wyllie (1975) Water content of a granite magma deduced from the sequence of crystallization determined experimentally with water-undersaturated conditions. *Contrib. Mineral. Petrol., 52,* 175–191.

Moore, J. G. and J. P. Lockwood (1973) Origin of comb layering and orbicular structure, Sierra Nevada batholith, California. *Geol. Soc. Am. Bull., 84,* 1–20.

Mustart, D. A. (1969) Hydrothermal synthesis of large single crystals of albite and potassium feldspar (abstr.). *Trans. Am. Geophys. Union, 50,* 675.

——— (1972) *Phase Relations in the Peralkaline Portion of the System* Na_2O-Al_2O_3-SiO_2-H_2O. Ph.D. Thesis, Stanford University, Stanford, California.

Naney, M. T. (1977) *Phase Equilibria and Crystallization in Iron- and Magnesium-bearing Granitic Systems.* Ph.D. Thesis, Stanford University, Stanford, California.

Nockolds, S. R. (1954) Average chemical composition of some igneous rocks. *Geol. Soc. Am. Bull., 65,* 1007–1032.

Swanson, S. E. (1977) Relation of nucleation and crystal-growth rate to the development of granitic textures. *Am. Mineral., 62,* 966–978.

——— (1978) Petrology of the Rocklin pluton and associated rocks, western Sierra Nevada, California. *Geol. Soc. Am. Bull., 89,* 679–686.

———, J. A. Whitney, and W. C. Luth (1972) Growth of large quartz and feldspar crystals from synthetic granitic liquids (abstr.). *Trans. Am. Geophys. Union, 53,* 1127.

Turnbull, D. and J. C. Fisher (1949) Rate of nucleation in condensed systems. *J. Chem. Phys., 17,* 71–73.

Wager, L. R. (1959) Differing powers of crystal nucleation as a factor producing diversity in layered igneous intrusions. *Geol. Mag., 96,* 75–80.

Walker, D., R. J. Kirkpatrick, J. Longhi and J. F. Hays (1976) Crystallization history of lunar picritic basalt sample 12002: phase equilibria and cooling rate studies. *Geol. Soc. Am. Bull., 87,* 646–656.

Whitney, J. A. (1972) *History of Granodioritic and Related Magma Systems: an Experimental Study.* Ph.D. Thesis, Stanford University, Stanford, California.

——— (1975) The effects of pressure, temperature, and X_{H_2O} on phase assemblage in four synthetic rock compositions. *J. Geol., 83,* 1–31.

Wyllie, P. J. (1963) Applications of high pressure studies to the earth sciences. In R. S. Bradley, Ed., *High Pressure Physics and Chemistry,* vol. 2, p. 1–89. Academic Press, New York.

Yoder, H. S., Jr. (1950) High–low quartz inversion up to 10,000 bars. *Trans. Am. Geophys. Union, 31,* 827–835.

Manuscript received, June 18, 1979;
accepted for publication, December 21, 1979.